IL NUOVO CIMENTO **46 C** (2023) 57
DOI 10.1393/ncc/i2023-23057-2

COMMUNICATIONS: SIF Congress 2022

Issues in the experimental determination of electron screening effects in nuclear reactions of astrophysical interest

S. S. PERROTTA([1])([2])([3])

([1]) *Università degli Studi di Catania - Catania, Italy*
([2]) *Istituto Nazionale di Fisica Nucleare, Laboratori Nazionali del Sud - Catania, Italy*
([3]) *Universidad de Sevilla - Seville, Spain*

received 16 February 2023

Summary. — In fixed-target experiments at collision energies of astrophysical interest ($\lesssim$100 keV), the dynamics of nuclear reactions between charged particles is affected by electrons bound to the projectile and target. Some measurements involving atomic-like targets suggest deviations sensibly greater than theoretically expected for a screening effect due only to atomic electrons. This work aims to study more in depth the degree of compatibility of experimental data with standard atomic theory. Traditional methods to estimate screening effects from data are presented, discussing their strengths and limitations, and a different approach is proposed. It is underlined how empirical investigations on screening cannot be disentangled from the problem of modelling the low-energy bare cross-section. The study was applied to the $^6\mathrm{Li} + \mathrm{p} \rightarrow {}^3\mathrm{He} + \alpha$ reaction.

1. – Introduction

The cross-section of a nuclear reaction between charged particles at energies of astrophysical interest is dominated by the probability of overcoming the system's Coulomb barrier through quantum tunnelling. It is common to express the angle-integrated cross-section as a function of centre-of-mass energy, $\sigma(E)$, in terms of the *astrophysical S-factor*, defined as in ref. [1], eq. (1):

$$S(E) = \exp[2\pi\eta(E)]E\sigma(E) \quad \eta(E) = \alpha_e Z_1 Z_2 \sqrt{\frac{mc^2}{2E}}, \tag{1}$$

where $\eta(E)$ is the Sommerfeld parameter [2], Z_1 and Z_2 the reactants charge numbers, m their reduced mass, α_e the fine-structure constant and c the speed of light.

It is recognised theoretically (see, *e.g.*, ref. [3]) and observed experimentally (see [1,4-6] and references therein for just some examples) that such nuclear processes can be affected

by the screening operated by other electric charges found in the reaction environment. The observed variation in the cross-sections depends on the environment under study. This work is in particular concerned with the study of screening effects in standard fixed-target experiments performed with targets whose electronic structure can presumably be treated as approximately atomic (measurements regarding metallic and alloy targets, see for example ref. [5, 7], are thus not considered here). In this framework, experimental cross-sections for several reactions were found to require sensibly stronger screening effects than theoretically predicted. The problem has been discussed in several works, see [1, 4, 8-11] and references therein for some examples. The discrepancies might be an evidence of a shortcoming in the experimental procedures and/or the theoretical framework. Furthermore, the involved systems and regimes often play a role in astrophysical models (see again refs. [1, 8] for some examples). It is recognised that the experimental predictions on screening effects depend on the assumed energy trend of the bare cross-section [8], but extensive investigations in this direction are not common. It has been suggested that the aforementioned discrepancies may be the result of purely nuclear features, such as clustering [11] or deformations [12], affecting the sub-Coulomb bare cross-sections.

The goal of the present paper is to explore the issue through a purely phenomenological study, making use of the theoretical ingredients discussed in sects. **2** and **3**. Section **4** hosts a comparison of several methods to deduce information on screening from experimental reaction data, applied to the $^6\mathrm{Li} + \mathrm{p} \rightarrow {}^3\mathrm{He} + \alpha$ case. In sect. **4**·3 we propose an approach, slightly different than those found in the literature, explicitly geared toward testing the compatibility between data and theoretical predictions on screening. Concluding remarks are presented in sect. **5**.

2. – Theoretical description of screening effects

The cross-section of a nuclear reaction taking place within an interacting environment, σ_e, can be approximately connected with the "bare" cross-section for the corresponding process taking place in vacuum, σ_b, as

$$\sigma_e(E) = \sigma_b(E + U), \tag{2}$$

where U is called *screening potential*. The validity conditions of the approximation depend on the environment (see refs. [9, 13] for some general discussion). For the case of screening by atomic electrons, ref. [3], sect. 2, discusses that relative errors of the order of U/E can be expected on the estimated screened cross-section.

A treatment on the theoretical determination of the screening potential U for a given environment is beyond the scope of this paper. For the present purposes, it is sufficient to state that the adiabatic-limit potential for a pair of colliding Li and H atoms is 182 eV (ref. [3], table 4), which is thought to apply reasonably well also to molecular systems and insulator targets (see, *e.g.*, [5] and references therein). The adiabatic limit provides the theoretical expectation for U in the limit of small collision energy (where screening effects are most important), and it is expected to provide an upper bound at finite energy (ref. [3], sect. 1).

The information regarding the effect of screening on the cross-section can be encoded in the *enhancement factor* $f_e(E)$, defined as $\sigma_s(E)/\sigma_b(E)$, which can be rewritten using eqs. (1) and (2). For many systems of interest, and with the possible exception of

regions with sharp resonances, U is small enough that $S(E+U)/S(E) \approx 1$ with good approximation, causing the enhancement factor to become independent of σ_b:

$$f_e(E,U) \approx \frac{E}{E+U}\frac{\exp[2\pi\eta(E)]}{\exp[2\pi\eta(E+U)]}. \tag{3}$$

For $U/E \to 0$ one finds $f_e \to 1$. For instance, for a ^{6}Li + p reaction, $f_e - 1 < 1\%$ for $U = 182\,\mathrm{eV}$ and $E > 75\,\mathrm{keV}$, or $U = 300\,\mathrm{eV}$ and $E > 100\,\mathrm{keV}$.

3. – Bare cross-section parametrization

In addition to relevant experimental data and an adjustable model for screening effects, the other required ingredient for the study is a model constraint on the bare cross-section, which is normally described phenomenologically by adjusting it on data. If resonances can play a relevant role in the region of interest, they may be taken into account through a phenomenological R-matrix fit [14]. Otherwise, the bare cross-section is usually parametrised assuming that the corresponding S-factor is a polynomial in energy:

$$\sigma_b(E) = \frac{1}{E}\exp[-2\pi\eta(E)](S_0 + S_1 E + \cdots + S_n E^n), \tag{4}$$

where the set of coefficients S_i is fitted. The order of the polynomial, n, is chosen empirically. The flexibility of such model can be helpful to fit on data without too specific assumptions on the nuclear process, but may also cause some effect not related to the bare reaction to be reabsorbed. In particular, note that any finite (and internally consistent) set of data can be always reproduced with a polynomial of sufficiently high order. Conversely, there can be physical features in data that a polynomial of finite order would struggle to describe accurately (resonances are a typical example).

A different kind of phenomenological expression, useful for non-resonant processes, can be derived in terms of an approximation of the exact Coulomb barrier transmission coefficient [9]:

$$\sigma_b(E) = \frac{1}{E}\frac{kR}{|H_0^+(\eta,kR)|^2}A_0, \tag{5}$$

where $H_l^+(\eta,\rho)$ is the spherical outgoing Coulomb function for the orbital angular momentum l, with η as in eq. (1) [2]. R and A_0 are adjusted on data. This is just the penetrability factor for zero angular momentum appearing in the R-matrix theory [14]. The more constrained nature of this expression prevents the inclusion in σ_b of effects, both spurious and genuine, not accounted for by the underlying theoretical model.

In the limit of $E \to 0$, eqs. (4) and (5) show a similar trend. For testing purposes, we will also consider a variation of eq. (5) where η, only when computing $H_l^+(\eta,\rho)$, is expressed using an arbitrary value Z in place of Z_1Z_2: for values slightly different than the physical one, the function retains essentially the same trend, except in the limit of $E \to 0$ (see ref. [9], sect. 1.2.3.d for more discussion and a sample figure).

4. – Approaches for the experimental determination of the screening potential

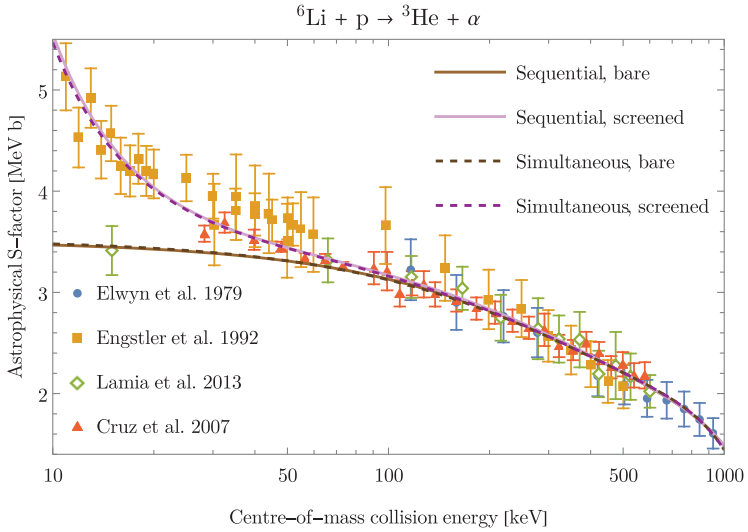

Fig. 1. – Green open diamonds represent the $^6\mathrm{Li} + \mathrm{p} \rightarrow {}^3\mathrm{He} + \alpha$ Trojan-Horse-Method astrophysical S-factor (see eq. (1)) from ref. [1]. All other points represent direct measurements from refs. [4,5,15] (see text for details). Lines represent the screened and bare S-factor fitted on data using either the "sequential" or "simultaneous" method (see tables I and III) as per the legend, with eq. (4) and $n = 3$.

4˙1. *"Sequential" fit of bare and screened cross-section.* – One way to study screening effects experimentally is to first of all obtain an estimation of the bare cross-section, σ_b, from data considered unaffected by screening, then subsequently compare it with direct measurements. The traditional approach (see, *e.g.*, ref. [4]) is to fit σ_b on data at relatively high collision energies, where screening effects become negligible (see eq. (3)), and extrapolating it to the region at lower energies. The extrapolation clearly introduces a dependence on the adopted model, whose associated uncertainty cannot be easily estimated. This can be mitigated if data from indirect measurements are taken into account. For instance, the green open diamonds in fig. 1 represent the astrophysical factor for the $^6\mathrm{Li} + \mathrm{p} \rightarrow {}^3\mathrm{He} + \alpha$ reaction obtained using the Trojan Horse Method in ref. [1]: the data extend down to very low collision energies but, differently than the other datasets in the figure (obtained from direct measurements), are not affected by screening effects. The improvement is limited by the uncertainty on indirect data, which, due to the way they are extracted, also bear some model dependence themselves ([1]).

After deducing the bare cross-section, the enhancement factor f_e, defined in sect. **2**, is found as the ratio of experimental cross-sections to the fitted bare trend. The uncertainty estimation on f_e is somewhat cumbersome in practice, as it is necessary to propagate the uncertainty on the fitted σ_b. Finally, eq. (3) is fitted on the estimated f_e, employing a constant screening potential U as free parameter. At this stage it is pointless to take into account the data previously employed for the bare cross-section fit. Another relevant but hard-to-estimate source of uncertainty is thus connected to the choice of the threshold

([1]) For instance, Trojan Horse absolute cross-sections are normalized to direct data at higher energies, and the energy trend is affected by the adopted assumptions on the bare Coulomb barrier penetrability.

TABLE I. – *Examples of "sequential" fits of the bare and screened cross-section, performed as described in sect.* **4**˙1*, using all data in fig. 1 and a threshold energy,* E_t*, of 100 keV. For each row, the table lists: the fitting function employed for* σ_b*, the predicted bare astrophysical factor at zero collision energy, the* χ^2 *and number of degrees of freedom for the* σ_b *fit, the predicted screening potential, and the* χ^2 *for the* f_e *fit, which included 34 data points and 1 free parameter.*

σ_b	$S_b(0)$[MeV b]	χ^2, DoF (σ_b)		U[eV]	$\chi^2(f_e)$
Eq. (4), $n = 1$	3.21 ± 0.05	18.9	47	536 ± 25	58.4
Eq. (4), $n = 2$	3.40 ± 0.08	9.9	46	430 ± 27	24.4
Eq. (4), $n = 3$	3.51 ± 0.13	8.9	45	379 ± 29	16.7
Eq. (4), $n = 4$	3.51 ± 0.20	8.9	44	382 ± 33	14.5
Eq. (5), $Z = 3$	3.45 ± 0.07	11.3	47	394 ± 26	20.7
Eq. (5), $Z = 2.98$	$+\infty$	13.5	47	258 ± 26	19.1

TABLE II. – *Same as table I ("sequential" method) but under different conditions. The first block of columns refers to fits performed using all data in fig. 1 and* $E_t = 75$ *keV. The last block of columns refers to fits performed using only data from refs.* [5, 15] *below 1 MeV (circles and triangles in fig. 1) with* $E_t = 100$ *keV.*

	All data, $E_t = 75$ keV		[5, 15] data, $E_t = 100$ keV	
σ_b	$S_b(0)$[MeV b]	U [eV]	$S_b(0)$[MeV b]	U[eV]
Eq. (4), $n = 2$	3.43 ± 0.07	410 ± 26	3.34 ± 0.09	530 ± 82
Eq. (4), $n = 3$	3.56 ± 0.12	354 ± 29	3.47 ± 0.18	367 ± 114
Eq. (4), $n = 4$	3.57 ± 0.19	351 ± 32	3.55 ± 0.34	292 ± 170
Eq. (5), $Z = 3$	3.47 ± 0.06	381 ± 26	3.42 ± 0.07	375 ± 76

energy E_t at which direct data are assumed to represent bare cross-sections, and thus employed to fit σ_b rather than f_e. Note that the precise energy at which screening becomes important depends on U itself, whose estimation is the very purpose of the analysis under discussion.

As an example, the "sequential" approach was here applied to experimental data in fig. 1 for the $^6\mathrm{Li} + \mathrm{p} \to {}^3\mathrm{He} + \alpha$ reaction ([2]). For illustration, fig. 1 includes both the bare and screened astrophysical factors fitted in this manner for one case. More results are reported in tables I and II, which also include a comparison of calculations performed adopting different threshold energies E_t. Despite there being only 3 data points from direct measurements in fig. 1 at energies between 75 keV and 100 keV, the difference in the predicted screening potential when setting E_t to either value is quite sizeable.

As a measure of the fit quality, the associated total χ^2 and number of degrees of freedom are reported in table I. Only for eq. (4) with $n = 1$, the fit on f_e yields an unacceptable χ^2, suggesting either the need of a non-constant screening potential or, more simply, that the linear model is too poor to adequately describe the data.

([2]) Data in refs. [1, 15] are taken from `www-nds.iaea.org/exfor`. Data in ref. [5] are taken from tables 5.4 and 5.8. Data in ref. [4] are taken from table I; the "normal kinematics" data, which were normalized to older measurements, are in disagreement with the inverse-kinematics datasets in the same table, thus, for simplicity, they were not included here. For all datasets, all quoted uncertainty sources for data were added quadratically.

TABLE III. – *Example of simultaneous fits of the bare and screened cross-section, performed as described in sect.* **4**˙2*. The first column lists the fitting function employed for* σ_b*. The first block of columns refers to fits performed on all data in fig. 1, and lists the predicted bare astrophysical factor at zero collision energy,* $S_b(0)$*, the predicted screening potential,* U*, and the* χ^2 *of the fitted model with respect to only the 11 data points in fig. 1 at energies above 500 keV. The last block of columns refers to fits performed using only data from refs.* [5, 15] *below 1 MeV (circles and triangles in fig. 1) and lists the corresponding* $S_b(0)$ *and* U*.*

	Data from refs. [1, 4, 5, 15]			Data from refs. [5, 15]	
σ_b	$S_b(0)$ [MeV b]	U [eV]	$\chi^2_{E>500\,\mathrm{keV}}$	$S_b(0)$ [MeV b]	U [eV]
Eq. (4), $n = 1$	3.35 ± 0.02	449 ± 31	11.0	3.27 ± 0.04	617 ± 96
Eq. (4), $n = 2$	3.45 ± 0.03	392 ± 33	2.6	3.41 ± 0.05	410 ± 112
Eq. (4), $n = 3$	3.52 ± 0.05	364 ± 37	1.9	3.52 ± 0.09	285 ± 135
Eq. (4), $n = 4$	3.55 ± 0.08	355 ± 42	1.9	3.60 ± 0.15	222 ± 166
Eq. (5), $Z = 3$	3.44 ± 0.03	391 ± 32	3.4	3.42 ± 0.05	367 ± 106
Eq. (5), $Z = 2.98$	$+\infty$	272 ± 32	4.5	$+\infty$	144 ± 106

The dependence of the results on the adopted bare-cross-section model can be observed comparing each line of tables I and II. Unsurprisingly, greater predicted zero-energy bare astrophysical factors correlate with smaller predicted screening potentials. Additionally, the uncertainties on the fit predictions increase with the number of free parameters: this is because an enlarged space of available models allows to attain the same total χ^2 with a greater interval of values for each specific prediction.

The fits performed using eq. (4) with $n \geq 3$ and eq. (5) with $Z = 3$ are compatible within one standard deviation. The predictions from eq. (4) with $n = 2$ are instead slightly incompatible with the others, even though the model fits data satisfactorily, and there does not seem to be a good reason to discard it. Such degree of agreement is a consequence of having chosen fitting functions for σ_b that, without strong constraints from data, tend to yield similar low-energy extrapolations. To provide an exaggerated but clear example of the model dependence of results on U, table I includes a fit performed using the alternate version of eq. (5) with $Z = 2.98$: here, a sensibly smaller screening potential is found, while keeping good overall agreement with data. Note how, without the constraint given by indirect data, any trend for σ_b at low energies would be acceptable, allowing for practically any value of U to be drawn. Direct data at very low energies are instead important to constraint U for a given σ_b. As an example, table II shows some fits performed using only data from refs. [5,15]. Lacking the aforementioned constraints, the uncertainty on U and $S_b(0)$ rises significantly, together with the magnitude of the differences between the best-fitting values for different fitting functions.

4˙2. *Simultaneous fit of the bare and screened cross-section.* – Some issues of the "sequential" approach discussed in sect. **4**˙1 can be circumvented if both the bare cross-section and the screening correction are fitted simultaneously on data at all energies. Table III shows the results of such analysis using the same data employed in sect. **4**˙1, and fig. 1 includes, for illustration, both the fitted screened S-factor and its bare part for one case. The screened cross-section was here modelled using directly eq. (2). In the literature, indirect measurements are usually excluded from such "simultaneous" fits, perhaps due to the technical difficulty of fitting two different but coupled models (namely, on the bare and screened cross-section) on distinct datasets. In the present

work, this was achieved by formally treating the dataset kind (direct or indirect) as an additional predictor.

Compared to the "sequential-method" case, the analysis is here computationally more demanding, but has a simpler workflow. More importantly, this simultaneous approach removes the issue of the choice of an energy threshold E_t mentioned in sect. **4**˙1, and allows to constraint the model (especially the low-energy bare cross-section) better, making full use of the information given by all data. Additionally, fitting both σ_b and f_e simultaneously takes more explicitly into account the interdependence between the two quantities (which exists regardless of the adopted analysis method), in the form of correlations between the fit parameters: a wider range of U can yield fits of similar quality if the bare cross-section is adjusted accordingly in each case (within the constraints given by data), and vice versa. In accordance with these expectations, the predicted zero-energy bare astrophysical factors have a smaller uncertainty in table III than in tables I and II, while the screening potentials have a somewhat greater uncertainty in table III.

The comparison between predictions from different bare-cross-section models shows the same qualitative features discussed in sect. **4**˙1. Here, the fit total χ^2 is quite good for all models compared to the number of degrees of freedom. More detailed information can be obtained considering the χ^2 accrued on specific energy regions (or on different datasets). In particular, table III reports, for some cases, the χ^2 associated to only the data points at energies between 0.5 and 1 MeV: the value is rather poor (but not enough to reject the fit) only when using eq. (4) with $n = 1$.

As already found in sect. **4**˙1 for the sequential method, if the simultaneous fits are repeated using only data from refs. [5,15], the predicted screening potentials, reported in the last block of table III, show both greater uncertainties and greater absolute variations among different fitting functions for σ_b.

For each specific model for σ_b, the absolute difference between the best-fitting values of U in tables I and III, using the sequential or simultaneous method, can be quite important, typically of the same order of magnitude of the uncertainty assigned to each value ($\sim$10%) when using eq. 4. It is at the same time interesting to notice that, except for eq. (4) with $n = 1$, the S-factor predictions in tables I and III are compatible within about 1% (see also fig. 1 for a graphical comparison of one case). The conclusion seems to hold even if relevant data is removed from the fit (compare the fits performed using only data from refs. [5, 15] in tables II and III). We believe the same applies to the comparisons in ref. [10].

4˙3. *Compatibility of data with pre-determined screening model.* – The traditional methods discussed in sects. **4**˙1 and **4**˙2 are mostly concerned with characterising the *best-fitting* screening model. However, one of the main goals of the experimental analyses on atomic screening effects is often just to determine whether measured screened data are compatible with theoretical expectations for such effects. Here, we thus suggest to adapt the analysis approach to focus on this goal, by explicitly testing the hypothesis that screening is described by a given model ([3]). From the technical point of view, the method is quite similar to the simultaneous approach in sect. **4**˙2, and mainly differs for the focus shift from best-fit estimates to p-values.

A first comparison between direct and indirect data covering overlapping energy re-

([3]) A mention of calculations performed in a similar spirit was found in ref. [10], which quotes the total χ^2 of some fits performed assuming a fixed value of U.

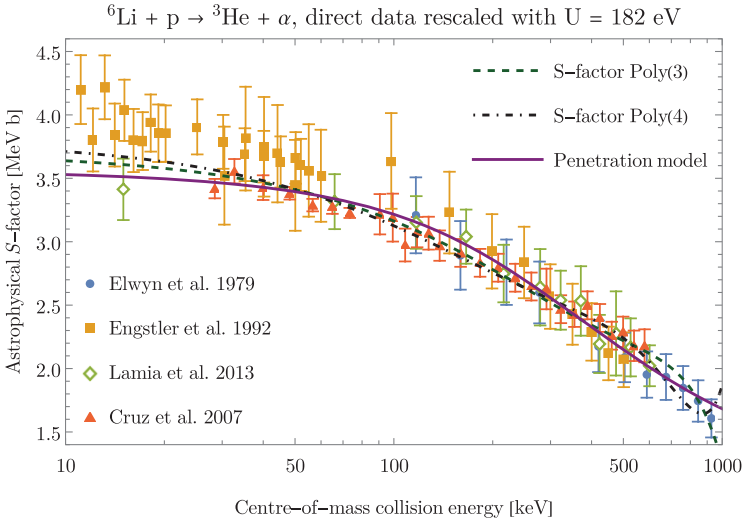

Fig. 2. – Example of study of experimental data using a pre-determined assumption for screening effects. Green open diamonds are THM data from ref. [1]. All other points are the same direct data in fig. 1 from refs. [4, 5, 15], as per the legend, but rescaled using eq. (3) with $U = 182\,\mathrm{eV}$. Lines are best fits to displayed data: "S-factor Poly(n)" and "Penetration model" in the legend refer, respectively, to eq. (4) and eq. (5) with $Z = 3$.

gions might be performed without the need of any further assumption. Upon fixing a prescription for $U(E)$ it is sufficient to employ eq. (3) to factor out the assumed screening enhancement from the direct data, obtaining an estimate for the bare cross-section. As an example, fig. 2 shows the same data in fig. 1 but with all points from direct measurements rescaled by the enhancement factor corresponding to $U = 182\,\mathrm{eV}$ (see sect. **2**). There is apparent tension between data from ref. [4] at the lowest collision energies and the first data point from ref. [1], which differs by more than 1 standard deviation, but less than 2, from the weighted average of the same data point and data from ref. [4] below 20 keV ([4]). This is an expression of the fact, already seen in sects. **4**˙1 and **4**˙2, that the adopted data tend to favour a stronger screening. Despite this, since the discrepancy is due to a single data point, it is not sufficient to confidently exclude the compatibility of data with the assumed screening model.

In order to make use of the full set of data in the analysis, it is necessary to put a constraint on the bare cross-section trend, allowing to fit eq. (2) on data with a fixed value for U. If the adopted model for σ_b is assumed to be correct, a poor fit could then be attributed to an inadequate choice of U. If, on the contrary, data and model show no tension and the chosen U has a solid theoretical backup, the fitted σ_b may be a better estimate than the one obtained following sects. **4**˙1 and **4**˙2. Some information on the quality of the model for σ_b, at least with regards to under-fitting, might be gathered by comparison with data not affected by screening. For instance, eq. (4) with $n = 1$ (not shown here) might be discarded on this basis.

From the practical point of view, after choosing U and the model for σ_b, eq. (2) is

([4]) There is some tension also between data from refs. [4, 5]. However, both datasets are drawn from direct measurements, and the sort of modelling considered here cannot solve this kind of discrepancy.

TABLE IV. – *Example of a study of the range of screening potential values compatible with experimental data. Each row lists the fitting function employed for σ_b, together with the corresponding range of screening potentials passing the test described in sect.* **4**˙3 *under different conditions. The column headers specify the energy threshold E_t adopted in each case. The last column refers to calculations including only data from refs.* [5,15] *below 1 MeV, while for the other columns all data in fig. 1 were employed.*

	Compatible U [eV]		
σ_b	$E_t = 100\,\mathrm{keV}$	$E_t = 75\,\mathrm{keV}$	[5,15] data, $E_t = 75\,\mathrm{keV}$
Eq. (4), $n = 2$	257 to 503	266 to 498	70 to 623
Eq. (4), $n = 3$	215 to 503	224 to 497	−76 to 618
Eq. (4), $n = 4$	176 to 521	183 to 513	−224 to 677
Eq. (5), $Z = 3$	268 to 506	277 to 500	85 to 622

fitted on data, including those not affected by screening. This helps to constraint σ_b. The total χ^2 of the fit is however not very meaningful to quantify the agreement with screened data, as it includes a significant contribution from other data as well. Thus, adapting the standard approach for χ^2 hypothesis testing (see, *e.g.*, ref. [16]), we consider the fit χ^2 due only to the d data points obtained from direct measurements at energies below a given threshold E_t. We will reject the hypothesised model, at confidence level L, when the cumulative distribution function of the chi-square distribution with d degrees of freedom, $F_d(x)$ for brevity, is such that $F_d(\chi^2) > L$. We set $L = \mathrm{erf}(1/\sqrt{2})$ ("one sigma") to perform a fair comparison with the other results reported in this work ([5]).

As an example, fig. 2 includes the best fit, on all data in the same figure, of three different models for σ_b. As will be shown below, assuming $U = 182\,\mathrm{eV}$, eq. (5) with $Z = 3$ and eq. (4) with $n \leq 3$ can be rejected according to the criterion given above, while eq. (4) with $n \geq 4$ provides an acceptable (in the above sense) description of screened data: note how table III could have been interpreted as suggesting the contrary. For a more elaborated application, table IV shows, in several cases, the interval of values of U which, if assumed to represent the correct screening potential, would pass the aforementioned criterion. We believe that this kind of intervals are, in the present context, of greater interest compared to the uncertainties on U in table III, which instead only concern the fluctuations of the best-fitting parameter.

Within the present approach, greater values of E_t usually yield wider intervals of acceptable values of U, as seen here in table IV. This is because data at higher collision energies is less affected by screening, but the current approach "weights" equally the χ^2 due to each data point.

To comment again on the importance of employing data at very low energies in the analysis, table IV shows that measurements from refs. [5,15] alone allow for a much wider interval of acceptable screening potentials. In particular, $U = 182\,\mathrm{eV}$ is compatible with

([5]) The stated criterion does not take into account that fitting the bare cross-section on data removes some degrees of freedom. However, σ_b is more prominently constrained by data not affected by screening, and it is not trivial to deduce the correct distribution to assume for the residuals of interest. For the illustrative purposes of the present work, the aforementioned approach is deemed sufficient.

all tested models for σ_b, and $U = 0$ is compatible with eq. (4) at $n \geq 3$. Hence, such dataset, in itself, is not sufficient to discriminate screening effects with enough confidence. New measurements in the energy range first covered in ref. [4] could be extremely useful.

Finally, as was already found for the other analysis approaches in sects. **4**˙1 and **4**˙2, the results in table IV can change sensibly with the fitting function adopted for σ_b, with less constrained functions allowing for wider intervals of screening potential values.

5. – Conclusions

After an in-depth study of the analysis approaches commonly employed in the literature to extract information on screening effects from experimental reaction data, in sect. **4**˙3 we proposed an alternative method, deemed to better address the question of compatibility between data and theoretical expectations. Here, the idea was implemented as a simple χ^2 hypothesis test, but more sophisticated approaches could be employed as well.

Regarding the role of experimental data, it was seen to be necessary to provide screened cross-sections with small uncertainty compared to the expected screening: this also implies that measurements at lower collision energies tend to be more relevant. It is also important to take into account both indirect and direct data not affected by screening, to constraint the bare-nucleus cross-section, σ_b.

With the exception of the comparison discussed at the beginning of sect. **4**˙3, all the analysis methods taken into account in this work depend on the choice of a fitting function for σ_b. Within the approaches in sects. **4**˙1 and **4**˙2, the fitted value of "U" does not represent the actual screening potential unless σ_b is correct. The approach proposed in sect. **4**˙3, instead, only tests the compatibility of a given model for σ_b with data under the assumption that the screening model is the correct one, or the other way around. Determining whether a given model for σ_b is accurate (or at least physically reasonable) would require a more microscopical investigation of the process. Hence, within an empirical study, explicit checks on the model dependence of results on screening can be helpful to understand the robustness of the conclusions.

* * *

The author would like to thank C. Spitaleri and A. Bonasera for the important contributions given to the motivations of this work and its implementation, as well as M. Colonna and J. A. Lay for the useful discussions related to the ideas discussed here. This project received funding from the European Research Council under the European Union's Horizon 2020 research and innovation program (grant agreement No. 714625).

REFERENCES

[1] Lamia L. *et al.*, *Astrophys. J.*, **768** (2013) 65.
[2] Thompson I. J., `https://dlmf.nist.gov/33.22`.
[3] Bracci L. *et al.*, *Nucl. Phys. A*, **513** (1990) 316.
[4] Engstler S. *et al.*, *Z. Phys. A*, **342** (1992) 471.
[5] Cruz J., PhD Thesis (Universidade NOVA de Lisboa) 2006.
[6] Cruz J. *et al.*, *J. Phys. G*, **35** (2007) 014004.
[7] Cruz J. *et al.*, *Phys. Lett. B*, **624** (2005) 181.
[8] Adelberger E. G. *et al.*, *Rev. Mod. Phys.*, **83** (2011) 195.
[9] Perrotta S. S., PhD Thesis (University of Catania and University of Seville) 2022.

[10] Barker F. C., *Nucl. Phys. A*, **707** (2002) 277.
[11] Spitaleri C. *et al.*, *Phys. Lett. B*, **755** (2016) 275.
[12] Perrotta S. S. *et al.*, *Nuovo Cimento C*, **45** (2022) 123.
[13] Perrotta S. S. and Bonasera A., *Nucl. Phys. A*, **989** (2019) 168.
[14] Descouvemont P. and Baye D., *Rep. Prog. Phys.*, **73** (2010) 036301.
[15] Elwyn A. J. *et al.*, *Phys. Rev. C*, **20** (1979) 1984.
[16] Loreti M., *Teoria degli Errori e Fondamenti di Statistica*, 2006, https://wwwcdf.pd.infn.it/labo/INDEX.html.